3

Electrical Characterizations of Lead Free Sr and Sn Doped $BaTiO_3$ Ferroelectric Films Deposited by Sol-Gel

Jean-Claude Carru, Manuel Mascot and Didier Fasquelle
Univ. Lille Nord de France, ULCO
France

1. Introduction

Ferroelectric materials (FM) are known for a long time ago but it is only recently that they have been deposited in the form of thin films with a thickness typically inferior to 1 μm. The electrical properties of FM are now used to realize electronic components (Uchino, 2010), thanks to the high quality of ferroelectric thin films. Their main electrical properties are :

- high dielectric permittivity ε′
- tunability of ε′ under a DC field E_{DC} : ε′(E)
- non linear polarization P showing an hysteresis cycle : P(E)
- pyroelectric and piezoelectric behaviours

$PbZrTiO_3$ (PZT) is the most used material from a commercial point of view. In fact it has numerous applications such as piezoelectric actuators and transducers, infrared sensors, capacitors, RAM memories, MEMS, etc…However, its main disadvantage is to contain lead with regards to the European directive RoHS (Restriction of Hazardous substances, 2002/95/CE) which prohibits, since july 2006, different polluting materials in electronic components like lead. However lead oxides based FM are still used for their superior piezoelectric properties, but in a near future they will be banned. The search to find an alternative to PZT has begun before the RoHS directive but that concerned mainly the ceramic form. To the best of our knowledge, up to now, no lead free ferroelectric ceramic has superior or even equal piezoelectric performances to PZT.
The chapter contains 5 paragraphs devoted to: material aspects (elaboration and physical characterizations), dielectric, ferroelectric, pyroelectric and piezoelectric, I (V) characterizations of our doped $BaTiO_3$ thin films (either BST or BTS). In the conclusion, their properties will be compared with the ones of PZT films deposited on the same substrate.

2. Materials

The crystallographic structure was characterized by X-Ray θ/2θ diffraction using a Rigaku Miniflex+ diffractometer (filtered $CuK_{\alpha 1}$ radiation, λ = 1.5406 Å).
The morphology of the films was determined using Scanning Electron Microscopy (SEM) with a LEO438 VP apparatus. The thickness of the films was measured both by SEM and

with a TALYSURF INTRA150 profilometer. The typical thickness of our BTS films is about 400 nm.
The electrical properties were determined at room temperature in the frequency range 20 Hz-10^6 Hz as a function of a DC bias (- 40 volts, + 40 volts) with an Agilent HP4284A impedance analyzer coupled to low frequency Cu/Be microprobes from Signatone. The polarization cycles, pyroelectric current and piezoelectric coefficient d_{33} were recorded at room temperature with home-made automated systems.

2.1 Sol-gel deposition

$BaTiO_3$ films doped with Strontium (BST) were prepared from alkaline acetates $Ba(CH_3COO)_2$, $Sr(CH_3COO)_2$ and Ti-isopropoxide $Ti(C_{16}H_{28}O_6)$. Acetic acid ($C_2H_4O_2$) and 2-propanol ($CH_3CHOHCH_3$) were used as solvent agents. Barium acetate and strontium acetate were mixed according to a predetermined ratio of 90/10 and then added in the acetic acid solution. This solution was heated up to 120 °C for 1h. After cooling down to room temperature, Ti isopropoxide was added. Finally 2-propanol was added to control the solution concentration to 0.2 mol%. The final solution was deposited by spin coating at 2500 rpm during 20 s for each layer which was then dried at 300°C for 1 min (Vélu et al, 2003). After deposition of 7 layers, each sample was annealed in air in a tubular oven and these operations were repeated until the wanted final thickness was obtained. BST thin films were deposited by a sol-gel process on commercial (100) silicon wafers from CRYSTAL GmBH with the following layers : 1µm SiO_2 / 40 nm Ti / 200 nm Pt sputtered. Finally gold has been evaporated through a shadow mask to realize the upper electrodes with circular dots ranging from 150 µm to 2 mm in diameter. The Pt layer acted as bottom electrode. The upper electrode diameter was measured by an Olympus BX60 optical microscope.
For $BaTiO_3$ films doped with Tin (BTS), the process was identical to the BST one. The only change concerns dibutyltin oxide $C_8H_{18}OSn$ instead of strontium acetate $Sr(CH_3COO)_2$.
The doping of $BaTiO_3$ with Strontium leads to a substitution of Barium by Strontium (in A site) while the doping by tin entails a substitution of Titanium by Tin (in B site). So, the chemical composition of our BST and BTS films are as follows:

$$BST = Ba_{0.9}Sr_{0.1}TiO_3 \; ; \; BTS = BaTi_{0.98}\,Sn_{0.02}O_3$$

2.2 Crystallinity

Figure 1 shows the XRD patterns for the BTS thin films annealed at 750 °C for 1 hour (a) and at 950 °C for 15 minutes (b). The films are well crystallized and the perovskite structure is identified. A polycrystalline growth is evidenced for the two films. A change of the orientation from 750 °C to 950 °C is clearly seen with the appearance at 950 °C of the (100) and (111) BTS peaks. Moreover, the large increase of the (110) BTS peak indicates the preferential (110) plane orientation when increasing the annealing temperature to 950 °C. It is a proof of the crystallinity improvement when increasing the annealing temperature. We also observe that the width of the perovskite peaks decreases for the film annealed at 950 °C : this is linked to an increase of the grain size. This fact along with the improvement of the crystallinity will have a favourable effect on the dielectric permittivity and on the ferroelectric properties as will be shown later on (see § 3.1 and 4.1).

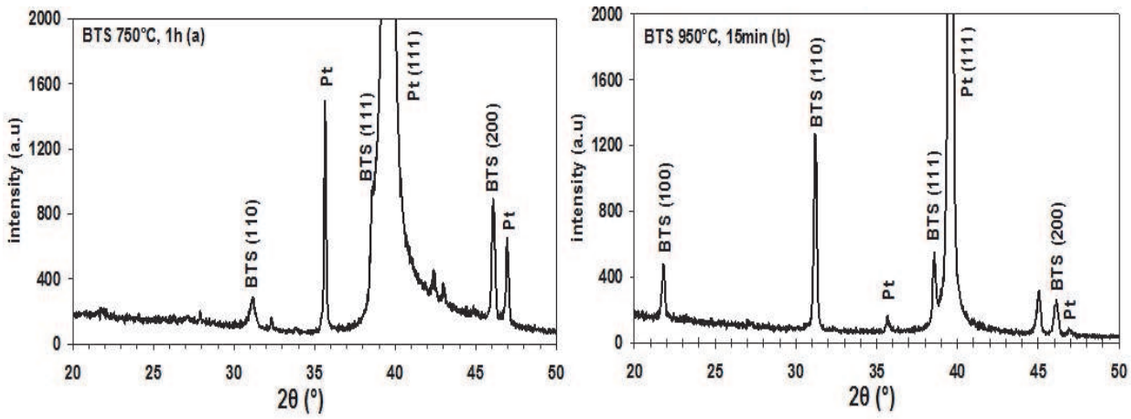

Fig. 1. XRD patterns of BTS thin films annealed at 750 °C during 1 h (a) and at 950 °C during 15 min (b).

2.3 Microstructure

Figure 2 is a SEM micrograph of the films annealed at 750 °C for 1 h (a) and at 950 °C for 15 min (b). We can see a substantial increase of the size of the grains for the film annealed at 950 °C. The mean grain size of this film is about 110 nm against 60 nm for the film annealed at 750 °C. This increase is in agreement with our XRD patterns and with other results on BST films (Malic et al, 2007). Moreover, the surface observation shows a rather good density of grains without cracks.

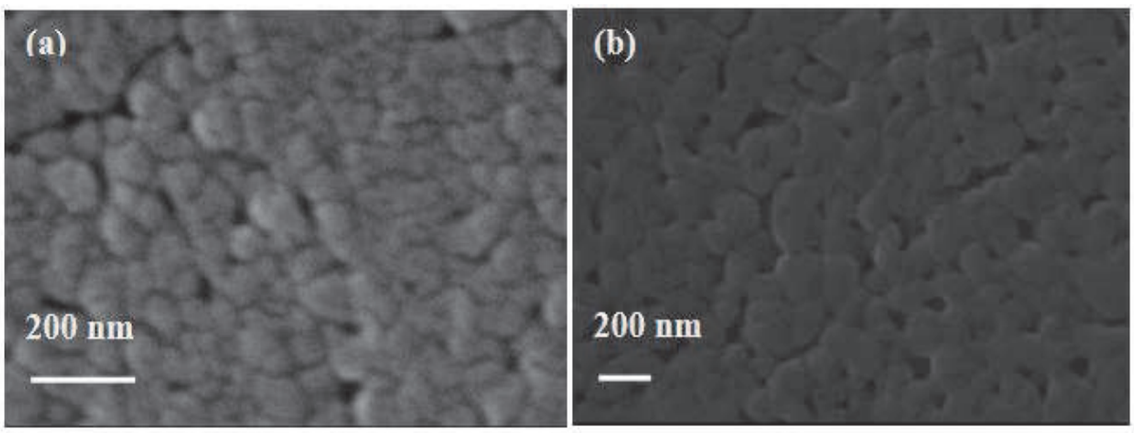

Fig. 2. SEM photographies of BTS thin films annealed at 750 °C during 1 h (a) and at 950 °C during 15 min (b).

3. Dielectric characterizations

The dielectric characterizations consist in determining the complex permittivity ε^* as a function of frequency and temperature :

$$\varepsilon^*(F,T) = \varepsilon'(F,T) - i\varepsilon''(F,T) \quad (1)$$

where ε' is the dielectric permittivity, ε'' is the dielectric losses and the ratio $\varepsilon''/\varepsilon' = tg\delta$ is the loss tangent.

In this section we present the influence : of the annealing conditions of the films, of the thickness of the films and of the substrates. The ferroelectric-paraelectric transition is also studied.

3.1 Influence of the annealing

Annealing of the samples is necessary to crystallize the BST and BTS films in the perovskite structure (Agarwal et al, 2001). Two parameters are important to study : the temperature and the duration of the annealing.

3.1.1 Effect of the temperature

The dielectric permittivity ε′ and loss tangent tgδ responses of the BST thin films annealed at 750 °C, 850 °C and 950 °C during 1 hour are shown as a function of frequency in figures 3a and 3b respectively. It can be noted that for the three samples ε′ decreases in the entire frequency range and in the same manner. For example, the relative decrease ε′(1 kHz) – ε′(1 MHz)/ε′(1 kHz) is equal to about 8 %. This dispersion effect is commonly observed on ferroelectric films and has been attributed to the film-electrode interface effects and domain walls motions. It can be noted that ε′ increases when the annealing temperature increases : indeed, from 750 °C to 950 °C, ε′ for example at 10 kHz has evolved from 330 to 530 which corresponds to a relative increase of 60 %. This significant evolution can be attributed to the increase of the size of the grains and of the enhancement of density. It is in agreement with results obtained on barium titanate ceramics (Arlt et al, 1985; Frey et al, 1998). Previously, we have measured similar values of the dielectric constant for $Ba_{0.8}Sr_{0.2}TiO_3$ films annealed at 750 °C (Mascot et al, 2008).

As concerns the loss tangent presented figure 3.b, for the three samples the curves are very close and merge at 1 MHz towards a value inferior to 0.01. This value is similar to a published one for PZT deposited by a sol-gel route (Sun et al, 2003). We observe for the three samples a decrease of the losses when the frequency increases. So, we could anticipate that the decrease of dielectric losses when increasing the frequency is encouraging for radiofrequencies and microwaves applications.

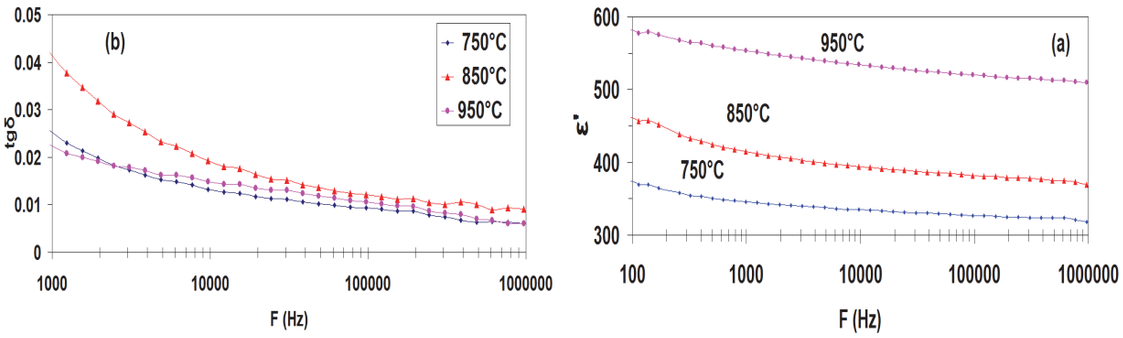

Fig. 3. Dielectric permittivity (a) and loss tangent (b) for BST films annealed at 750 °C, 850 °C and 950 °C during 1 h in air.

3.1.2 Effect of the duration

We present in figure 4 the evolution of the dielectric permittivity for BST films annealed at 950 °C during different durations. It can be seen that above 1 kHz the dielectric permittivity

increases when the annealing duration decreases. For example at 1 MHz the values of ε′ are 500, 720 and 830 for duration respectively of 1h, 30min and 15mn. Moreover the film annealed during 15 min has a low value of the loss tangent tgδ = 0.01 at 1MHz.

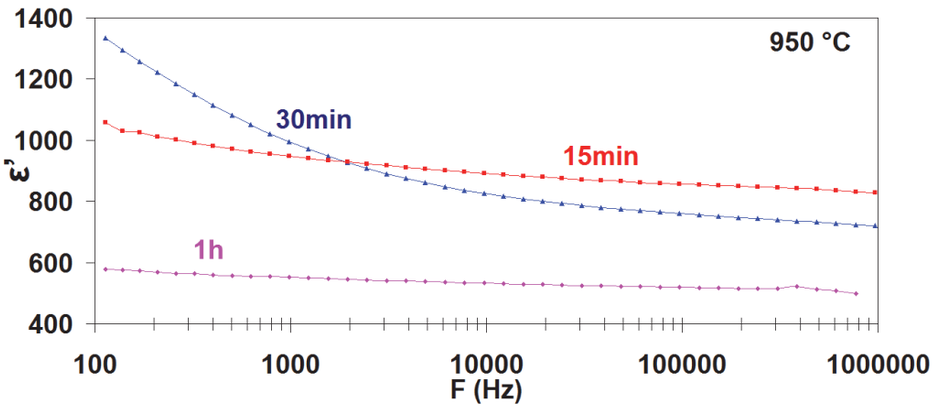

Fig. 4. Dielectric permittivity for BST thin films annealed in air at 950 °C during 15 min, 30 min and 1h.

Then a short time of annealing in air during 15min and at 950°C is most favourable for the dielectric properties.

3.1.3 Microwave annealing

We have made an annealing in a microwave oven (Keyson et al, 2007) at 750 °C during 5 min for a BTS film, 400 nm thick deposited on a Si/Pt substrate. The XRD pattern is presented figure 5.a. It can be compared with one of a BTS film annealed at 750 °C during 1 h in a tubular oven shown figure 1.a. The two BTS films are polycrystalline without preferential orientation whatever the type of annealing. However, with an annealing by microwaves, the amplitude of the peaks is higher and moreover the (100) orientation is observed. So, the crystallisation with a common microwave oven is rather good. It is very interesting as the energy budget is largely inferior to the one with a tubular oven and also as regards the cost, a microwave oven is quite inexpensive.

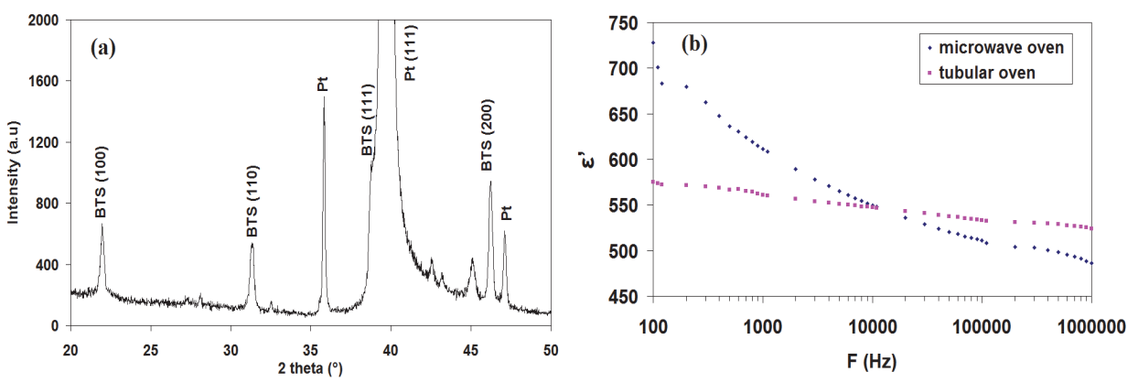

Fig. 5. XRD of a BTS film annealed at 750 °C in a microwave oven (a) and dielectric permittivity of this film and of a BTS film annealed at 750 °C in a tubular oven (b).

The dielectric permittivity measured at room temperature is presented figure 5.b. From 100 Hz to 10 kHz the dielectric permittivity is higher with the microwave annealing whereas it is inferior above 10 kHz. It can be observed that the frequency dispersion is much higher with the microwave annealing than with the conventional one. For example between 100 Hz and 1 MHz it is (728 - 486)/728, i-e 33 % for the microwave annealing and (575 - 524)/575, i-e 9 % for the conventional one annealed at 750 °C, 1 h. As concerns the loss tangent, not shown here, it is higher with a microwave annealing : tgδ = 0.04 at 1 MHz whereas it is only 0.01 with a conventional annealing. Nevertheless, the dielectric properties of a BTS film annealed at 750 °C during 5 min in a microwave oven are very encouraging.

3.2 Influence of the thickness

This study has been made on four BST films with thicknesses varying from 0.4 µm to 1 µm. The dielectric permittivity of these films is presented figure 6.a. We can see that above 1 kHz the dielectric permittivity increases with the thickness. This effect was also observed on a $Ba_{0.7}Sr_{0.3}TiO_3$ film (Parker et al, 2002). In figure 6.b the evolution of ε′ at 1 MHz is presented as a function of the thickness : a linear increase is evidenced from 0.4 to 0.8 µm and then ε′ tends towards saturation at 1 µm.

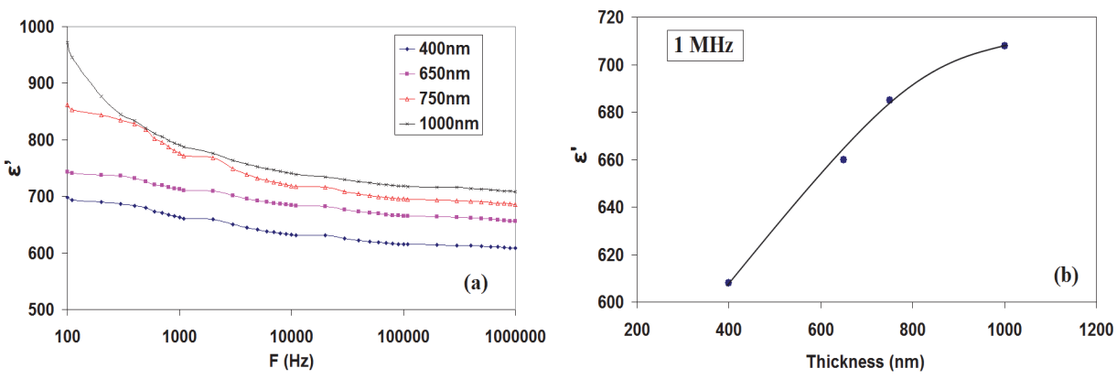

Fig. 6. Dielectric permittivity for four BST films as a function of frequency (a) and at 1 MHz (b) as a function of their thickness.

The increase of the dielectric permittivity can be well explain by the existence of a double layer : a layer with BST material and interface layers (Zhou & Newns, 1997) at the bottom and upper electrodes. These two interface layers are considered in the following as constituting only one interface layer. In fact, the effect of the interface at the bottom Pt electrode is higher than the one at the upper electrode interface due to the deposition conditions. So the measured inverse capacitance $1/C_{meas}$ is the sum of the inverse capacitance interface layer $1/C_i$ and of the BST capacitance layer 1/CBST as follows:

$$1/C_{meas} = 1/C_i + 1/C_{BST} \quad (2)$$

where $1/C_i=h_i/S\varepsilon_0\varepsilon_i$ and $1/C_{BST}=h_{BST}/S\varepsilon_0\varepsilon_{BST}$ with h_i and h_{BST} respectively the thickness of the interface and of the BST layers, ε_i and ε_{BST} the dielectric permittivity respectively of the interface and of the BST layers, S is the area of an electrode dot (250 µm in diameter). The evolution of $1/C_{meas}$ at room temperature and at 100 kHz is given figure 7 as a function of the thickness "h" of the films with:

$$h = h_i + h_{BST} \quad (3)$$

The curve obtained is a straight line, as for other authors (Cho et al, 2005) and whatever the measurement frequency. So, it means that the thickness h_i of the interface is negligible compared with the thickness h_{BST} of the BST layer. Then, if we consider in a first approximation that $h \sim h_{BST}$:

$$1/C_{meas} = 1/C_i + h/S\varepsilon_0\varepsilon_{BST} \quad (4)$$

So, from the slope of the straight line, we can calculate the dielectric permittivity of the BST layer : a value of $\varepsilon_{BST} = 844$ is obtained. Moreover, the extrapolation of the curve for h = 0 gives the value of $1/C_i$ which is about $4x10^8$ F^{-1}. With this value it is possible to estimate the thickness of the interface layer in nanometer : h_i (nm) = $0.18\varepsilon_i$. The value of ε_i is not known but surely inferior to ε_{BST} as, from a detailed study of the evolution of C_{meas} with a DC electric field (not discussed here), the interface is non ferroelectric (Chase et al, 2005; Mascot, 2009).
It has to be pointed out that some other effects can have an influence on the dielectric permittivity such as grain boundaries, mechanical strain at the interface with the substrate, internal stress and ferroelectric domains.

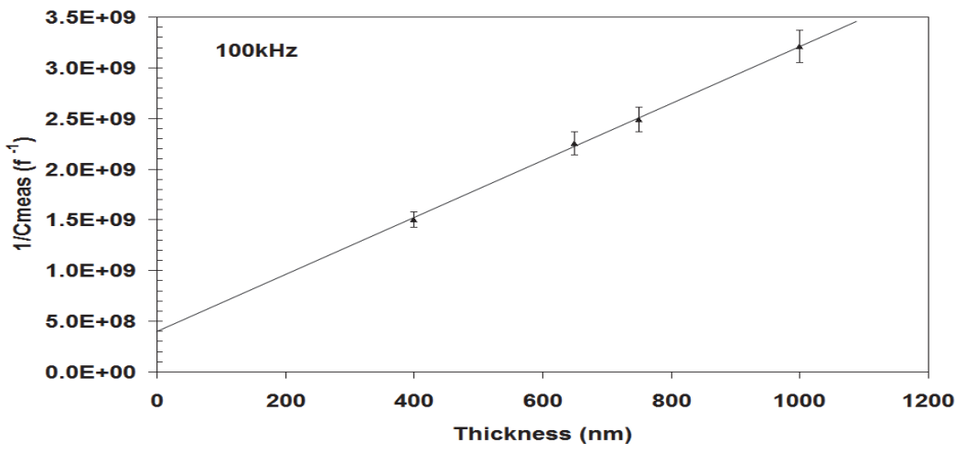

Fig. 7. Inverse of the capacitance at 100kHz for four BST films as a function of their thickness.

3.3 Influence of the substrate

We have deposited BST films, in the same conditions and annealed at 750 °C during 1 hour on stainless steel (type 304) and on platinized silicon substrates with a thickness of 400 nm. In figure 8 we present the evolution of the dielectric permittivity of these two films. It can be seen that the dielectric permittivity of the BST film is much higher with a Si/Pt substrate than with a steel substrate. In particular at 1 MHz, $\varepsilon' = 50$ with a steel substrate whereas it is 350 with a Si/Pt substrate. This can be explained by the existence of a large interface layer, which is not ferroelectric, between the steel substrate and the BST film. Then the capacitance C_i associated to this interface is the dominant term of the measured capacitance C_{meas}. Nevertheless we will show later on (§ 4.2) that the BST film deposited on stainless steel exhibits ferroelectric properties. In order to improve its dielectric properties a buffer layer would be necessary.

We have also deposited BST films on monocrystalline substrates such as sapphire and MgO. The objective was to evaluate the dielectric properties in high frequencies in order to realize tunable microwave components. We give here only some references (Burgnies et al, 2007; Houzet et al, 2008, 2010; Khalfallaoui et al, 2010) concerning our work as it is out of the scope of this chapter which is focused on low frequencies from DC to 1 MHz.

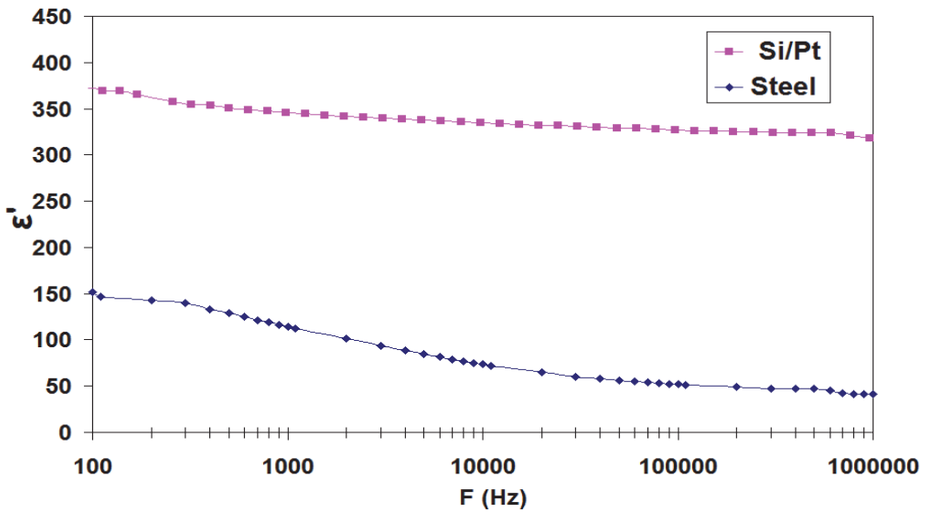

Fig. 8. Dielectric permittivity of BST films deposited on Si/Pt and stainless steel substrates annealed at 750 °C, 1h.

3.4 Ferroelectric-paraelectric transition

It has to be noted that T_C = +70 °C is independent of the duration of the annealing between 15 min and 1 h. The small variation of the dielectric permittivity between 20 °C and 70 °C may be interesting, for example, to realize electronic components such as integrated capacitors.

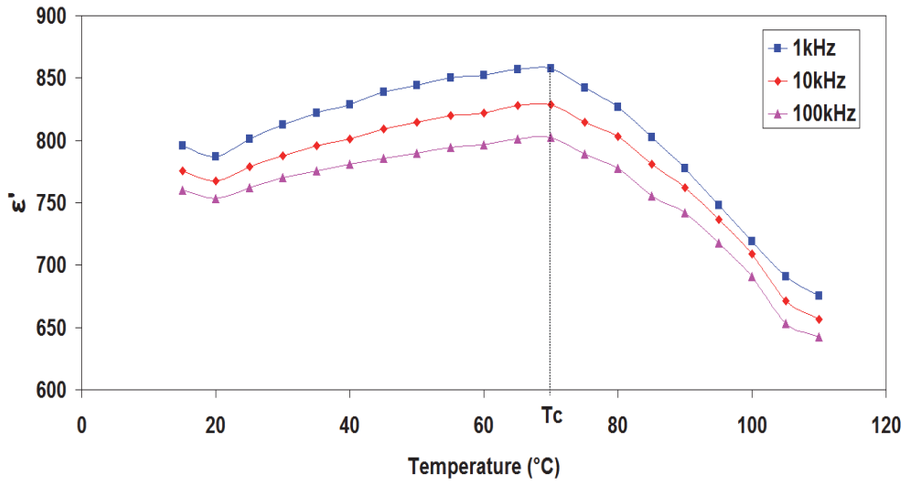

Fig. 9. Dielectric permittivity of a BST film at three frequencies as a function of temperature.

The evolution of the dielectric permittivity as a function of temperature is presented figure 9 for a BST film, 400 nm thick, annealed at 950 °C during 15 min. The plots are given at three frequencies : 1, 10 and 100 kHz. It can be seen that the shape of the three curves is exactly the same whatever the measurement frequency. A maximum is observed at T_C = +70 °C which corresponds to the ferroelectric to paraelectric transition. This transition is not as narrow as with BST in ceramic form : on BST films the transition is diffuse (Lorenz et al, 2003). Moreover, the T_C value is lower than the one found on a BST bulk material (Frayssignes et al, 2005) where Tc = +84 °C. This difference may be related to the small grain size (Frey et al, 1998; Parker et al, 2002) in a film compared with a ceramic and could also be due to a small difference of chemical composition as the transition temperature is very sensitive to Ba/Sr ratio.

4. Ferroelectric characterizations

Ferroelectric characterizations are made with two complementary techniques using a DC electrical field E_{DC} : capacitance measurement C(E) and hysteresis cycle recorded from polarization measurement P(E). These measurements are performed at the same medium frequency such as 1 kHz or 10 kHz.

4.1 Influence of the annealing

Different annealing conditions are studied on BST and BTS films, mainly the temperature and the duration of the annealing. Correlations are evidenced between the dielectric permittivity, the tunability and the size of the grains in the films.

4.1.1 Effect of the temperature

Figure 10.a shows the evolution at 10 kHz and room temperature of the capacitance as a function of a DC electric field for BST films annealed at different temperatures during 1 hour. The corresponding DC voltage variation was in the range [-5 V, +5 V]. The butterfly shape of the curves attests of the ferroelectric behaviour of these films because the polarization and capacitance vary non-linearly with the applied field due to the structure of ferroelectric domains. The shift on left of all these curves is due to the imbalance of space charges at the two different electrodes which may create an internal bias. In our case, BST was deposited on platinized silicon as bottom electrode and gold was used for the top electrode. This difference in metal used can explain the shift to the left of the curves. We also note on each curve a small difference in the height of the two peaks : this effect highlights the existence of a depletion layer capacitance. This depletion layer, also called previously "interface layer", was created between the ferroelectric film and the bottom electrode during the annealing stage. This interface layer, probably non ferroelectric, is due in our case to a diffusion process in our films at high temperature of metals (Pt, Ti) used as bottom electrode (Hu et al, 2006).
The tunability is defined by the following relation :

$$n_r = 1 - C_{min}/C_{max} = 1 - \varepsilon'(E_{max})/\varepsilon'(0) \quad (5)$$

For the annealing temperatures of 750°C, 850°C and 950°C during 1 hour, the tunability for a DC field of 125 kV/cm is about 30 %, 35 % and 63 % respectively. This property is very interesting for microwaves applications such as phase shifters, tunable filters and electronic antennas arrays.

The polarization cycles were recorded at room temperature also at 10 kHz. The three films showed hysteresis cycles with a quite symmetrical shape as can be seen on figure 10.b. We observe an increase of the remnant polarization when the annealing temperature increases. The remnant polarization P_r has evolved from 1 µC/cm² for an annealing at 750°C to 4.5 µC/cm² for an annealing at 950°C. This evolution is similar to the one of the dielectric permittivity previously observed for the different annealing temperatures (see Fig. 3). The presence of a remnant polarization confirms that our films are in a ferroelectric state. However our results are not as good as those for PZT films, P_r = 22 µC/cm² (Arlt et al, 1985) but they are similar to those for $Ba_{0.8}Sr_{0.2}TiO_3$ films, P_r = 5 µC/cm² (Mascot et al, 2008; Pontes et al, 2001).

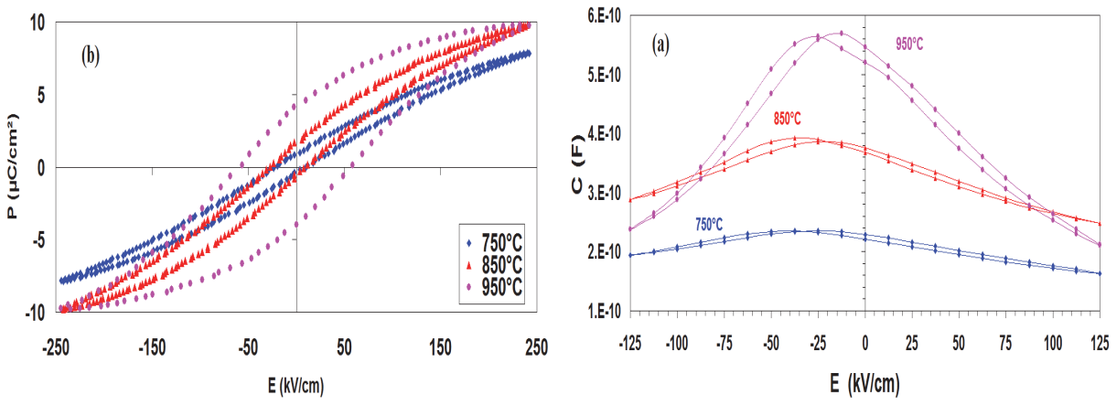

Fig. 10. Evolution at 10kHz as a function of a DC field of the capacitance (a) and of the polarization (b) for BST films annealed at 750 °C, 850 °C and 950 °C during 1h in air.

4.1.2 Effect of the duration

Figure 11 shows the evolution at 1 kHz of respectively the capacitance (a) and polarization (b) as a function of a DC field for 3 annealing duration at the optimum temperature of 950°C. It can be noted that the tunability exhibits a mean value of about 55% whatever the annealing duration. We observe that the C(E) plots of films annealed 15 min and 30 min are centred on the abscissa, while the film annealed 1 hour presents an hysteresis cycle shifted to the left. This shift was observed previously (see Fig. 10.a) on all films annealed during 1 hour. So, we infer that a shorter annealing time induces a lower diffusion process of (Pt, Ti) in the BST film. We think that a shorter annealing time has decreased the interfacial layer thickness because the C(E) curves became centred, showing that the internal bias has disappeared. The interest in a rapid thermal annealing is now well known for thin films and experimented with high power halogen furnaces. As shown previously for the dielectric properties, this minimized effect of the interfacial layer was also evidenced by a significant increased of the dielectric constant value (see Fig. 4**)**. In figure 11.b we observe on the hysteresis cycles that the remnant polarization is quite constant at 5 µC/cm² and also the coercive field at about 50 kV/cm when the annealing time decreases.

We have also studied the influence of the thickness for BST films annealed at 950 °C for 15min. In fact we have observed no effect neither on the tunability, nor on the remnant polarization for film thicknesses ranging from 0.3 µm to 1 µm.

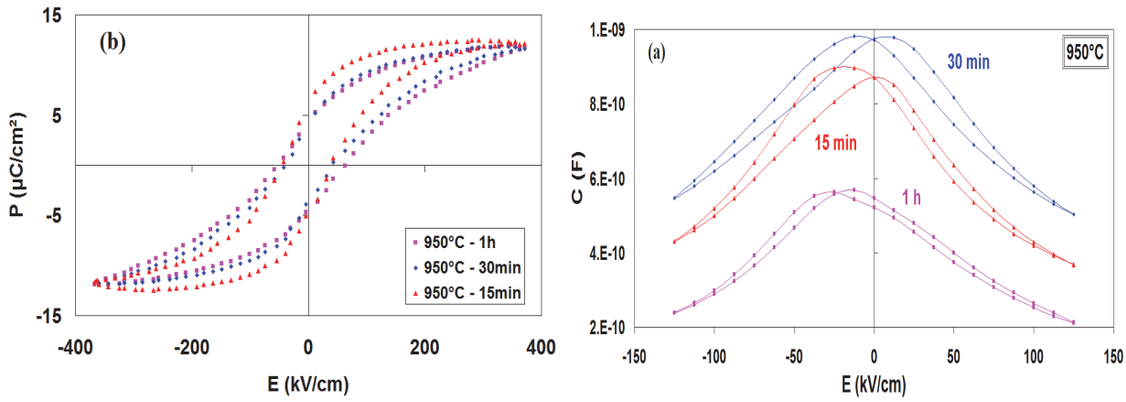

Fig. 11. Evolution at 1 kHz as a function of a DC field of the capacitance (a) and of the polarization (b) for BST films annealed at 950 °C during 1h, 30 min and 15 min in air.

4.1.3 Correlations

We present, figure 12.a , the evolution of the tunability at 10 kHz and of the grain size as a function of the dielectric permittivity for five different annealing temperatures and durations. It is clear that the grain size, the dielectric permittivity and the tunability increase when the annealing temperature increases from 750 °C to 950 °C during the same duration namely 1 hour. A similar evolution was also observed in the case of barium titanate ceramics (Frey et al, 1998). Conversely, at 950 °C, when the annealing duration decreases from 1 hour to 15 minutes, the grain size and the tunability remain constant to about 110 nm and 55 % respectively whereas the dielectric permittivity increases from 530 to 780. So, the annealing duration at 950 °C has no effect on the grain size with a maximum of one hour duration. This is in agreement with other works on BST thin films (Malic et al, 2007).

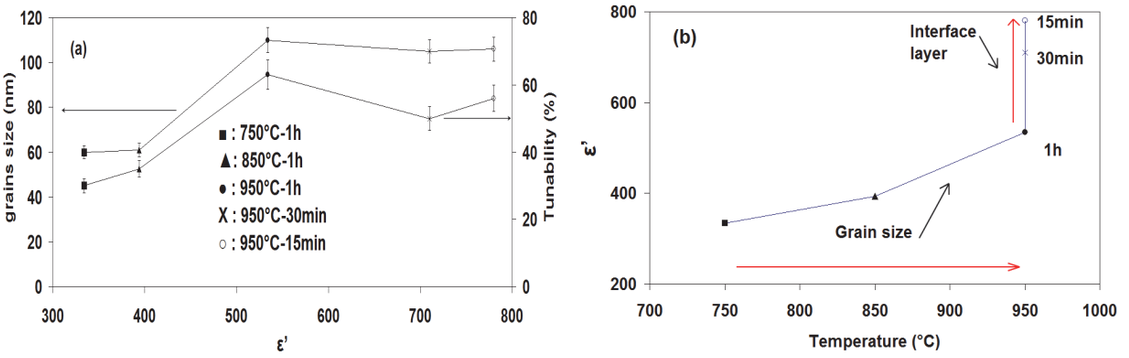

Fig. 12. Correlation of the tunability and of the grain size with the dielectric permittivity for BST films (a) evolution of ε' at 10 kHz as a function of different annealing conditions (b).

From figure 12.a we can see clearly that the tunability is correlated with the grain size. When the grain size increases, the number of grain boundaries decreases. Then, as the tunability increases markedly, this implies that these grain boundaries are non-ferroelectric. In the same way, figure 12.b, the continual increase of the dielectric permittivity can be attributed at first by the grain size increase and then to the interface layer thickness decrease. This is well interpreted by a brick-wall model (Mascot, 2009).

4.1.4 Effect of tin doping : BTS films

The evolution of the capacitance as a function of an electrical field E is given figure 13.a for two BTS thin films annealed at 750 °C during 1 hour and at 950 °C during 15 minutes. The DC electric field variation was in the range [-225 kV/cm; +225 kV/cm] and the measurement frequency was 10 kHz. The butterfly shape of the curves attests to the ferroelectric behaviour of the two films. The tunability for the annealing temperature of 750 °C@1 h is about 40 % and for an annealing 950 °C@15 min it is 76 % under a bias of +225 kV/cm. From figure 13.b it can be seen that for this field the tunability is close to its saturation value. To the best of our knowledge, the value of 76% is the highest reported for a doped $BaTiO_3$ thin film deposited by sol-gel (Mascot et al, 2011). Indeed, for example 45 % have been obtained but with a very high electric field of 400 kV/cm for a $BaSn_{0.05}Ti_{0.95}O_3$ film (Song et al, 2006). Our tunability of 76% corresponds to a variation by a factor 4 of the capacitance and by consequence of the dielectric permittivity. Such a variation can be well compared to the one of a varactor diode and is very interesting, as stated before, for the realization of tunable devices in radiofrequencies and microwaves.

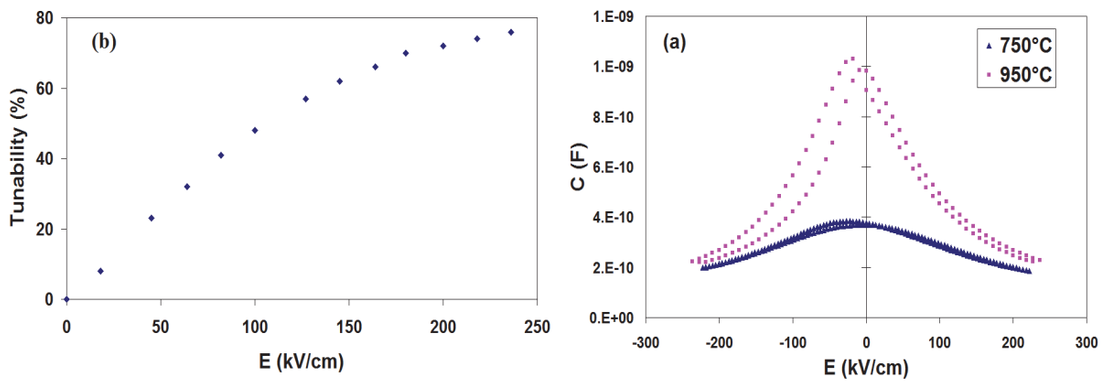

Fig. 13. Evolution at 10kHz of the capacitance as a function of a DC field for BTS films annealed at 750 °C and 950 °C (a) tunability evolution of the BTS film annealed at 950 °C.

4.2 Influence of the substrate

We study here the ferroelectric properties of BST films deposited on a low cost stainless steel substrate compared with the ones on higher cost Si/Pt substrates.

4.2.1 C(E) and hysteresis cycle

We consider the BST films deposited on stainless steel substrates on which we have made dielectric measurements (§ 3.3). In figure 14.a we present the evolution at 1 kHz of the reduced values of the capacitance as a function of a DC field for BST films deposited in the same conditions either on Si/Pt or stainless steel substrates and annealed at 750 °C during 1 hour. We can see that the tunability is largely inferior with the steel substrate than with the Si/Pt one. In fact it is only 9 % under a DC field of 250 kV/cm with a steel substrate whereas it is 30 % at only 125 kV/cm with a Si/Pt substrate. This shows that a thick non-ferroelectric interface layer is present between the BST film and the steel substrate. Consequently, the effective DC field applied to the ferroelectric BST layer is :

$$E_{DC}/(1+ C_{BST}/C_i) \quad (6)$$

with C_{BST} being the capacitance of the BST layer and C_i being the capacitance of the interface layer.
The hysteresis cycle figure14.b confirms the weak ferroelectric nature of the BST film deposited on stainless steel as the cycle is not saturated in comparison with the one of the BST film deposited on Si/Pt substrate.

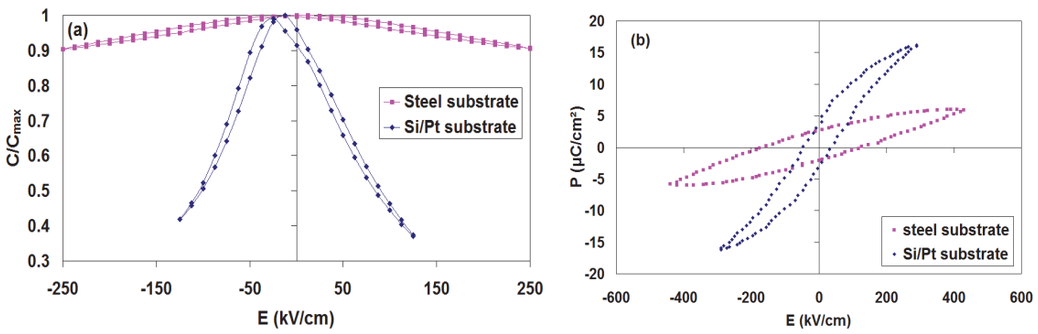

Fig. 14. Evolution at 1kHz as a function of a DC field of the reduced capacitance (a) and of the polarization (b) for BST films deposited on stainless steel and Si/Pt substrates.

4.2.2 Effect of an AC field

We have applied a variable AC field E_{AC} at a frequency of 10 kHz to the BST film deposited on stainless steel. Usually, for the dielectric measurements, the AC field applied is very small, typically 1 kV/cm. We can see, figure 15, that above this field and up to 50kV/cm, the dielectric permittivity has a constant value of $\varepsilon'(E_{AC}) = 50$. This behaviour characterizes a linear dielectric material : in our BST film it is due to the interface layer which is non-ferroelectric. However, above 50kV/cm, the dielectric permittivity increases : it is typical of a non-linear dielectric material. It is due here to the ferroelectric layer of the BST film. It is in relation with the Rayleigh law (Taylor & Damjanovic, 1998) **:**

$$E'(E_{AC}) = \varepsilon'(0) + \alpha' E_{AC} \tag{7}$$

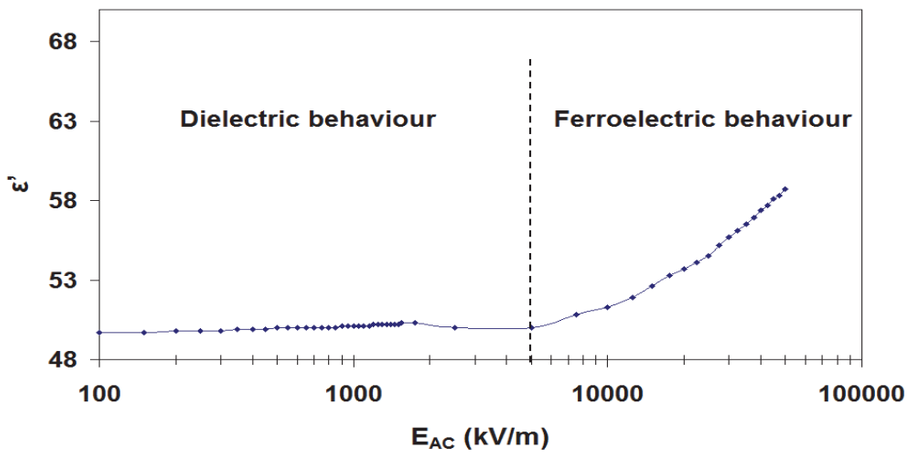

Fig. 15. Evolution at 10kHz of the dielectric permittivity as a function of an AC electrical field for a BST film deposited on a stainless steel substrate.

where ε′(0) is the dielectric permittivity without AC field and α′ is a constant linked to the movements of the ferroelectric domain walls under an AC field which increases the size of the domains. This confirms the existence of some ferroelectric domains in our sample. The increase of the dielectric permittivity is from a field of 50kV/cm which is at variance (not presented here) with a BST film deposited on Si/Pt substrate where the Rayleigh law is followed from a zero AC field with $\alpha' = 4.6 \times 10^{-5}$ m/V.
So, this study of the dielectric permittivity as a function of an AC field confirms both the existence of a major non ferroelectric interface layer and of ferroelectric domains in our BST film deposited on a steel substrate.

4.3 Paraelectric state

We have measured the evolution at 10 kHz and at a temperature of 100 °C of the capacitance under a DC field of a BST film annealed at the optimized temperature of 950 °C during 15 min. At this temperature the BST is in the paraelectric state as the curve C(E), figure 16.a, shows no (or a very small) hysteresis effect. We have fitted the corresponding dielectric permittivity following the Landau-Ginzbourg-Devonshire (LGD) model (Johnson, 1962) with the following formula :

$$\varepsilon'(E) = \frac{\varepsilon'(0)}{(1 + 12 C_3 \varepsilon_0^{\,3} \varepsilon'(0)^3 E^2)^{\frac{1}{3}}} \tag{8}$$

where ε′(0) is the dielectric permittivity without DC field and C_3 is a constant in the LGD model. C_3 was determined from our experimental results (Johnson, 1962; Outzourhit et al, 1995). The agreement is very good between the experimental values of $\varepsilon'(E_{DC})$ and the ones from the LGD model as can be observed figure 16.b. In fact, there is a maximum deviation of 2 %. So, from the LGD model, it can be seen that the dominant parameter for the tunability is the value of $\varepsilon'(0)^3 C_3$. A high value of the dielectric permittivity at zero field ε′(0) is then favourable to obtain a high tunability.

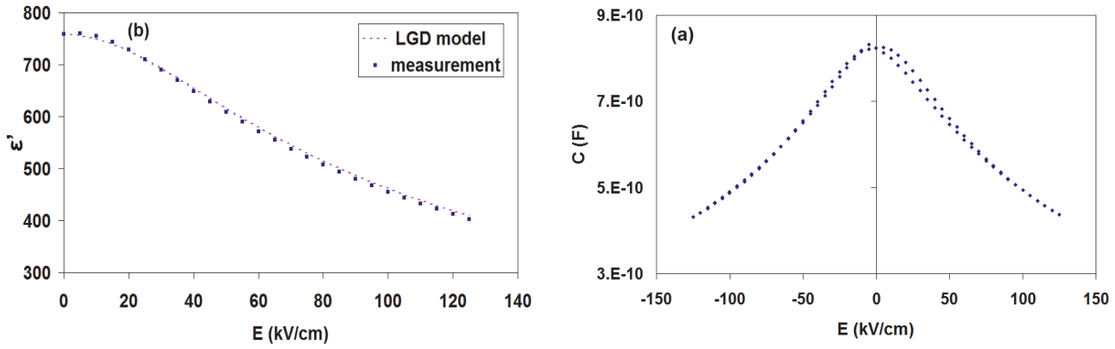

Fig. 16. Evolution at 10 kHz and 100 °C as a function of a DC field of the capacitance (a) and of the dielectric permittivity fitted with LGD model (b) for a BST films annealed at 950 °C.

5. Pyro and piezo-electric characterizations

In the ferroelectric state, contrary to the paraelectric state, it is possible to test the pyroelectric and piezoelectric properties : it is important in view of realizing sensors and actuators.

5.1 Pyroelectric characterizations

The pyroelectric coefficient γ has been determined from the measurement of the pyroelectric current I_p following the Bayer-Roundy method (Bayer & Roundy, 1972) leading to :

$$I_p = \gamma S \, dT/dt \tag{9}$$

where S is the electrode area, dT/dt is the rate of change of the temperature. This rate is sinusoidal as shown in figure 17a, thanks to a Peltier module. The magnitude of the pyroelectric current, figure 17a, is very low, typically some picoAmps. We have calculated a value γ = 140 μC/m²K at +25 °C for a BTS thin film annealed at 950°C during 15 min.

We present figure 17.b the evolution of the pyroelectric coefficient γ as a function of temperature for two BTS films annealed at 750 °C during 1 h and at 950 °C 15 min. We can see that the pyroelectric coefficient γ varies linearly, in a first approximation, with temperature. For the BTS film annealed at 950 °C@15 min, it increases for example from 140μC/m²K at +25 °C to 240μC/m²K at +100 °C which is an increase of 70 %. For the BTS film annealed at a lower temperature of 750 °C@1h, the pyroelectric coefficient γ is inferior by a factor of 1.4. So, the pyroelectric properties confirms that the dielectric (see figure 3.a) and the ferroelectric (see figure 10.b) properties are much better with an annealed at 950 °C than at 750 °C. For the two BTS films the pyroelectric coefficient γ reaches a maximum for a temperature of +105 °C which corresponds to the ferroelectric to paraelectric transition.

In order to realize sensors for example, it is necessary to determine the figure of merit defined (Zhang & Ni, 2002) as :

$$FOM = \gamma / d\varepsilon' tg\delta \tag{10}$$

with d being the thickness of the film. For example, for a BTS film (annealed at 950 °C@15 min) with a thickness of 0.4 μm, we obtain 40 μC/m³K at 10 kHz and +25°C. This value compares well with published data on BST films (Liu et al, 2003).

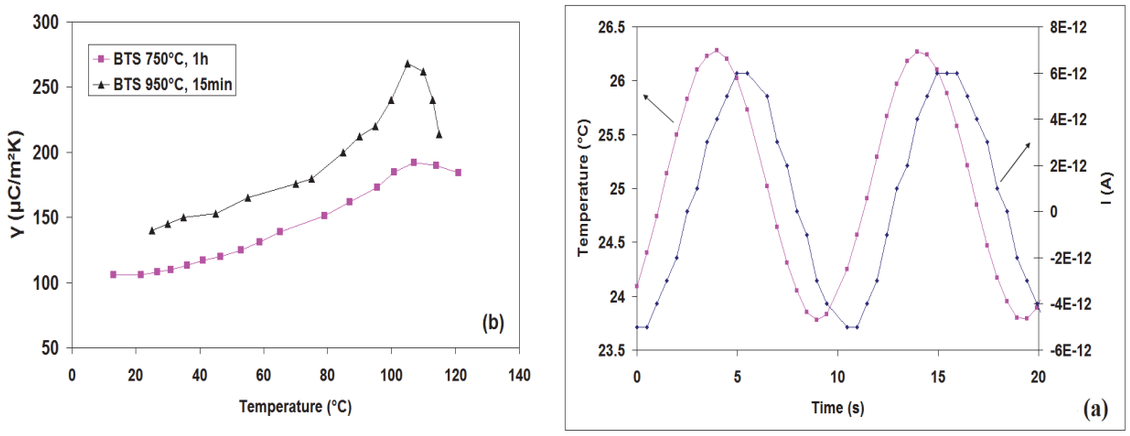

Fig. 17. Temperature and pyroelectric current as a function of time (a) pyroelectric coefficient versus measurement temperature (b) for two BTS films.

5.2 Piezoelectric characterizations

These characterizations are presented on BST films at two different scales : macroscopic one at millimetre level and nanoscopic one at nanometre level.

5.2.1 Macroscopic scale

The piezoelectric properties are determined by tensors with terms d_{ij}. In the case of our doped $BaTiO_3$ films which have a tetragonal crystalline structure, the piezoelectric matrix is mainly characterized by the terms d_{31} and d_{33}. We have developed a set-up to measure d_{33} by modifying a method proposed in the literature (Lefki & Dormans, 1994). It consists in applying a variable force on the film to measure the resulting electrical charge. The d_{33eff} effective coefficient is the derivative of the electrical charge by the force as follows :

$$d_{33eff} = dQ/dF \tag{11}$$

In figure 18 we present, for a BST film of thickness 1µm, the evolution at room temperature of the electrical charge as a function of a force applied from 0 to 10 N. We obtain d_{33eff} = 19 pC/N and 85 pC/N for a 1 µm thick PZT film deposited on the same substrate. This last value is close to 100 pC/N obtained with the same measurement method also for a PZT film (Ren et al, 1997). So the piezoelectric coefficient for BST is about 4.5 less than the PZT one.

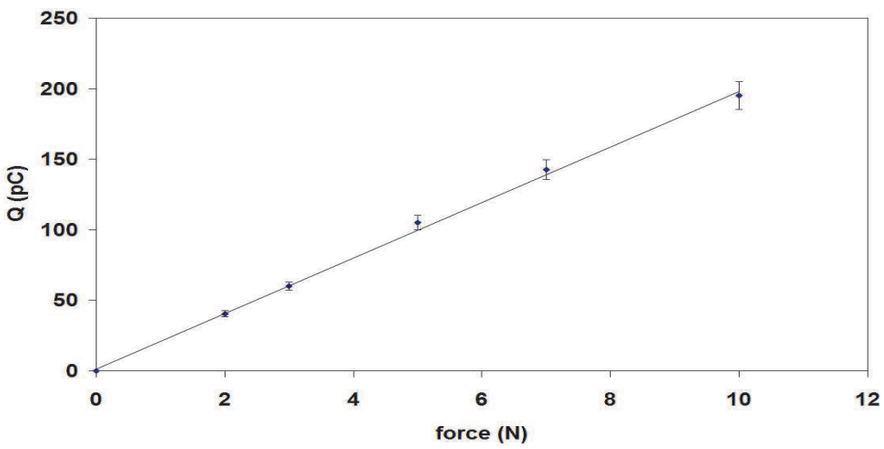

Fig. 18. Direct piezoelectric macroscopic response for a BST film, 1 µm thick.

5.2.2 Nanoscopic scale

Piezoelectric properties at the scale of a grain (size of about 110 nm) are determined by piezo force microscopy (PFM). The piezo response is obtained via the tip of the PFM which operates in contact mode. A DC field is applied between the tip and the bottom electrode of the film. A small AC field is applied to the tip in order to induce the vibration of the grain. We present, figure 19, the inverse piezoelectric response of a BST film deposited on Si/Pt substrate and annealed at 950 °C@15 min.

The magnitude, figure 19.a, represents the mechanical motion of the grain under a variable DC voltage between –10 volts and +10 volts. The butterfly shape of the curve attests of the ferroelectric and of the piezoelectric properties of the grain tested by PFM. The phase, figure 19.b, represents the switching of the electrical polarization of the grain from a negative DC field to a positive DC field and conversely. The hysteresis shape attests of the piezoelectric properties at the nanoscopic level of a grain. We can see that the phase change is about 160 ° which is close to 180 ° for a complete reversal of the polarization of the grain. It can be noted that the field necessary for the switching is 46 kV/cm which is very close to the value of the coercive field, i.e. 50 kV/cm of an hysteresis cycle at a macroscopic scale (see figure 11.b).

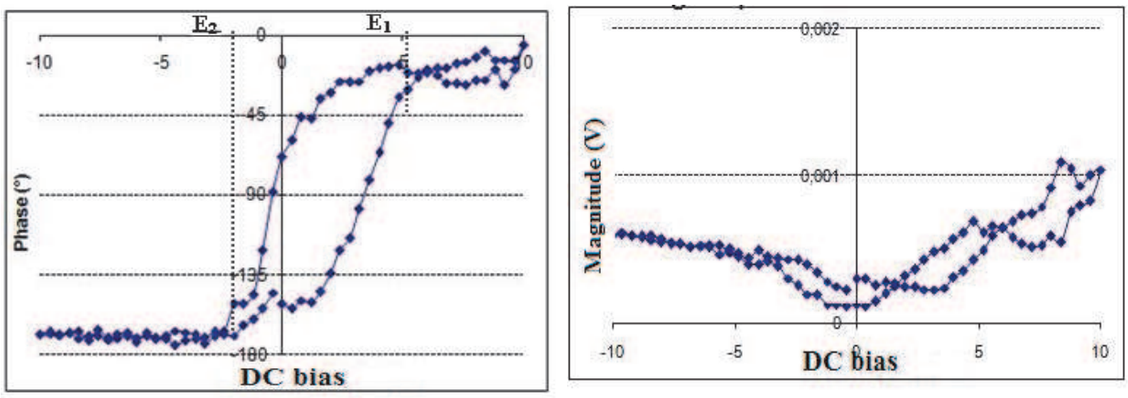

Fig. 19. Inverse piezoelectric nanoscopic response in magnitude (a) and phase (b) for a BST film.

6. J (E) characterizations

We have studied the current density J as a function of a DC field for BST and BTS films annealed at 950 °C during 15min. We present, figure 20, the evolution of J(E) in logarithmic scales for the two films under positive and negative bias. It can be seen that the conduction is very different with the two biases. For example, for the BTS film, J = 0.06 A/m² with E = +25 MV/m whereas J = 12 A/m² with E = -25MV/m. So, there is a ratio of 200 for these two current density which leads to a much higher leakage current with negative DC field bias. As with this bias the electrons come from the gold upper electrode, the electrical conduction is more important than with a positive bias for which the electrons come from the platinum bottom electrode. In order to explain that behaviour we have tested the different physical models of conduction available in the literature. They were mainly formulated for semi-conductor materials and adapted to ferroelectrics (Scott et al, 1991), namely Schottky barrier, Poole-Frenkel, Fowler-Nordheim and space charge mechanisms.

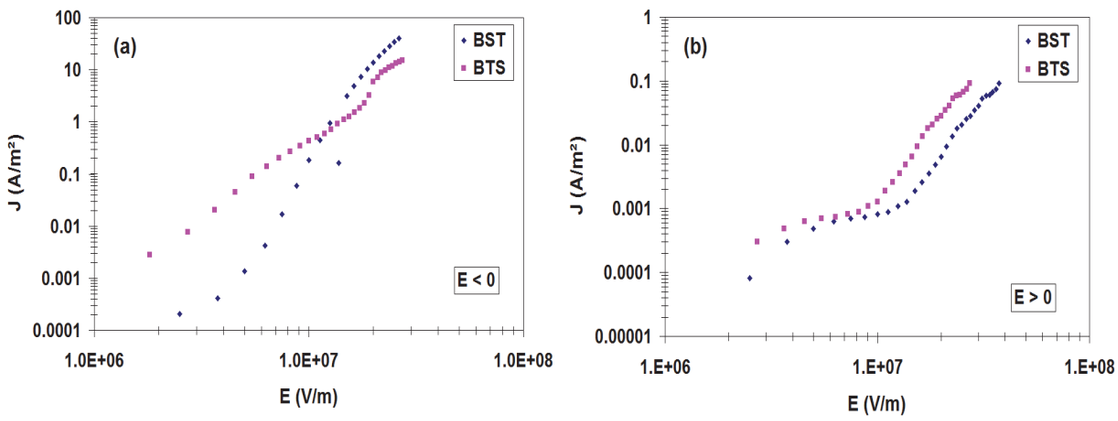

Fig. 20. Evolution of the current density as a function of a negative DC bias (a) and a positive DC bias (b) for BST and BTS films annealed at 950 °C during 15 min.

6.1 Schottky barrier

The Schottky mechanism is the major conduction mechanism at room temperature for ferroelectrics (Scott et al, 1991) from 1MV/m to some ten's of MV/m. The Schottky equation (Hwang et al, 1998) is as follows :

$$J = A^{*}\, T^{2} \exp\left[\frac{\beta_S\sqrt{E} - \varphi_S}{K_B T}\right] \tag{12}$$

with $A^{*} = (4\pi e m^{*} K_B^{2}/h^{3})$ where $e = 1.6\text{x}10^{-19}$ C, m* is the effective electron mass, K_B and h are the Boltzmann and the Planck constants, T is the temperature, $\beta_S = (e^{3}/4\pi\varepsilon_0\varepsilon)^{1/2}$ where $\varepsilon_0 = 1/36\pi\text{x}10^{9}$ F/m and ε is the dielectric permittivity at very high frequency, E is the applied DC field, φ_S is the Schottky barrier height.
It is useful to express $\log J/T^{2}$ as it varies linearly with $E^{1/2}$:

$$\log\frac{J}{T^{2}} = \frac{\ln A^{*}}{\ln 10} - \frac{\varphi_S}{K_B T \ln 10} + \frac{\beta_S}{K_B T \ln 10} E^{1/2} \tag{13}$$

In the following we will consider, as an example, the case of a BTS film.
A linear evolution of $\log J/T^{2}$ is observed only for a negative DC field as shown figure 21.a. We present also the measurement of the current density at different temperatures from 293 K to 393 K in order to determine φ_S. In this view, from the Schottky equation, we can express $\ln J/T^{2}$ as a function of 1/T as follows :

$$\ln\frac{J}{T^{2}} = \ln A^{*} + \left[\frac{\beta_S\sqrt{E} - \varphi_S}{K_B}\right]\frac{1}{T} \tag{14}$$

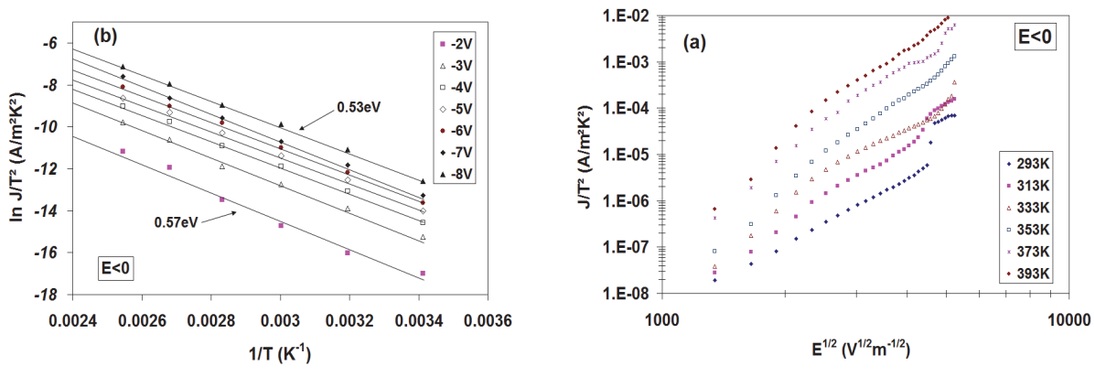

Fig. 21. Evolution of the current density as a function of a negative DC bias (a) and as a function of 1/T (b) for a BTS film.

We have replaced, figure 21.b, the DC electrical field E by V/d where V is the applied voltage and d is the thickness of the film, so $E^{1/2} = (V/d)^{1/2}$
The evolution of the activation energy E_A as a function of the applied voltage V is given by formula (15). The extrapolation, figure 22, at $V^{1/2} = 0$ volt gives the Schottky barrier height. Then we obtain $\varphi_S = 0.62$eV.

$$E_A\ (\text{eV}) = (-\varphi_S + \beta_S\sqrt{\frac{V}{d}}) \times \frac{1}{e} \tag{15}$$

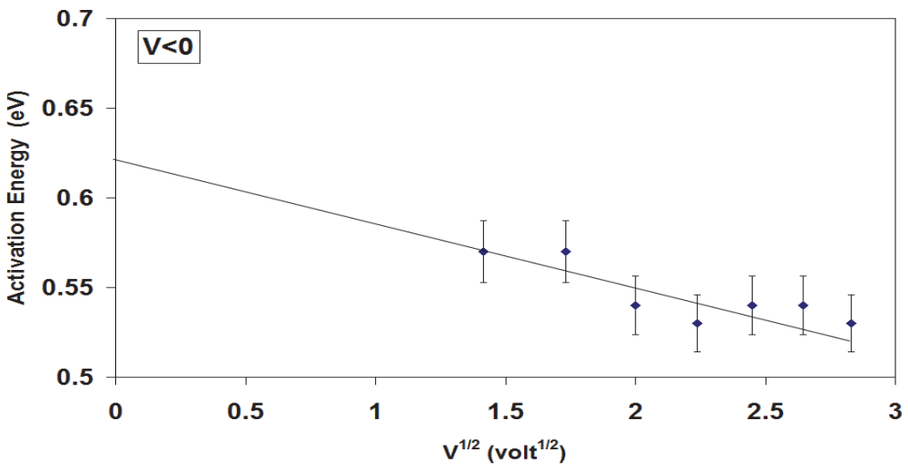

Fig. 22. Evolution of the activation energy as a function of a DC negative bias for a BTS film.

6.2 Space charge mechanism

The formula used to identify a space charge mechanism is a quadratic evolution of the current density as a function of the DC applied field as follows (Scott et al, 1991) :

$$J = aE + bE^2 \tag{16}$$

where « a » is a coefficient of ohmic resistivity in $\Omega^{-1}m^{-1}$ and « b » is a quadratic coefficient of space charge in $\Omega^{-1}V^{-1}$.

We show, figure 23, the evolution of the current density of the BTS film under an applied positive DC field. The experimental values follow, in a first approximation, the quadratic evolution of a space charge mechanism. With this model, the crossing of the tangents at low and high fields gives the threshold V_{TFL} « Trap Filled voltage Limit » beyond which the charges trapped are released. Then it is possible to calculate the number of traps N_t with the following formula (Chang & Lee, 2002) :

$$V_{TFL} = \frac{e d^2 N_t}{2\varepsilon_0 \varepsilon_r} \tag{17}$$

where e, d, ε_0 are defined previously and ε_r ~420 is the dielectric permittivity at low frequency for an applied voltage V_{TFL}. We have obtained $N_t = 1.27x10^{18}/cm^3$ for V_{TFL} = 8.25V. This value of N_t is comparable to a published one (Chang & Lee, 2002) on a BST film. We have calculated the energy of the traps : $E_t = E_c$ - 0.21 eV with the formulae proposed in the literature (Chang & Lee, 2002).

The mechanism of space charge is linked to the existence of free charges in the interfaces. It can be explained by two phenomena (Yang et al, 1998). The first phenomenon is the oxygen vacancies created at the interface of the BTS film and the platinum electrode during the annealing of the BTS film. The second phenomenon occurs when a DC field is applied. In fact oxygen ions can jump from the BTS grains in contact with the Pt electrode into this electrode. So, the lack of oxygen at the interface BTS film/Pt electrode creates a tank of oxygen vacancies. This oxygen vacancies tank contains free electron charges as shown by the following equation (Shen et al, 2002), at the origin of the leakage current:

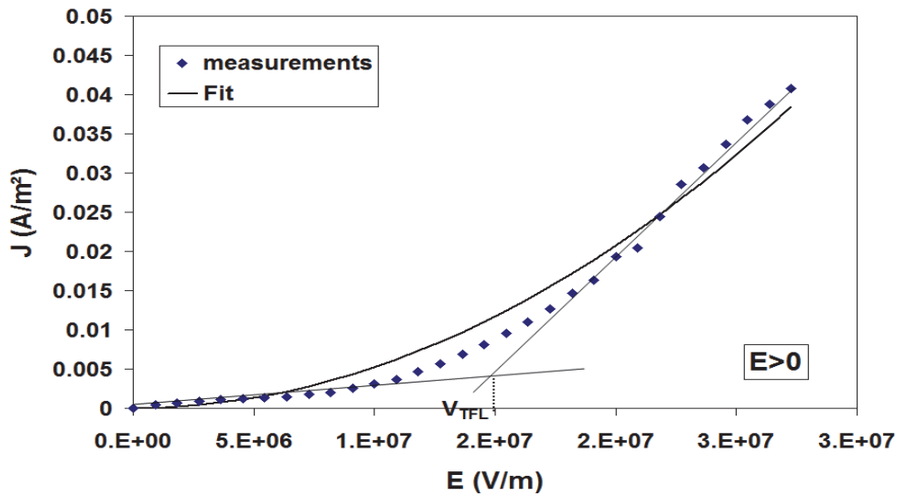

Fig. 23. Evolution of the current density as a function of a positive DC electrical field for a BTS film.

$$O_0 \rightarrow V_0^{2+} + 2e^- + 1/2O_2 \quad (18)$$

This study confirms the existence of an interface at the electrodes levels which was evidenced to be non ferroelectric by our dielectric measurements (§ 3.2).
That allows us to give figure 24 the energy band diagram for the BTS film with Pt and Au electrodes.

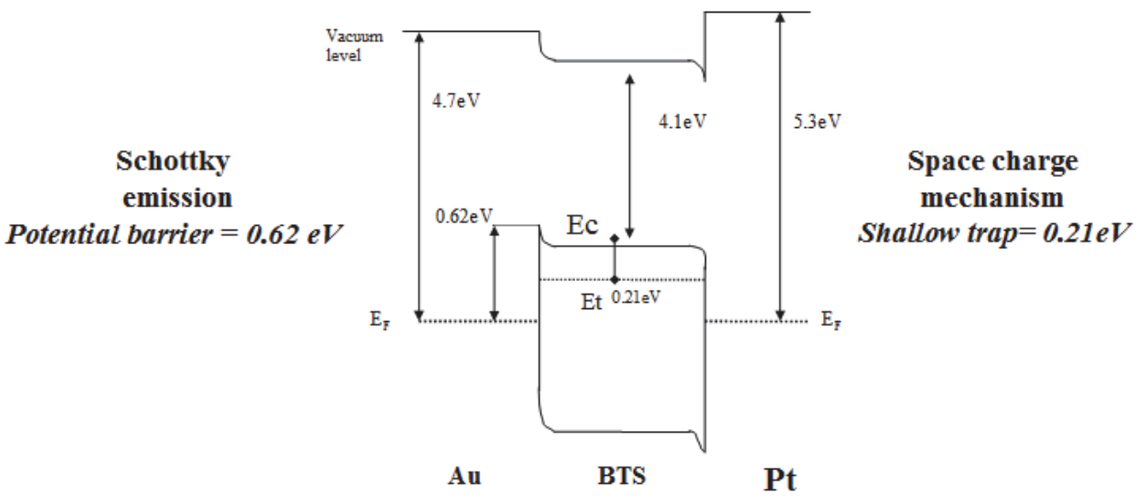

Fig. 24. Energy band diagram of a BTS film deposited on a Si/Pt substrate annealed at 950 °C during 15 min.

7. Conclusion

In conclusion, we have shown that it is possible to deposit by a low cost chemical technique, namely a sol-gel process, good quality ferroelectric films. They were derived from the

$BaTiO_3$ family by substitution with Strontium (BST) or Tin (BTS). We have improved the dielectric and ferroelectric properties by optimizing, first, the annealing conditions in air at 950 °C during only 15 minutes and second, the thickness of the films up to 1 µm. We have also shown that an annealing by microwaves at 750 °C during 5 minutes can crystallize the film in the perovskite structure and gives good dielectric properties. The electrical properties of BST and BTS films are better than the ones of the undoped $BaTiO_3$ films. For radiofrequencies and microwaves applications, the BST or BTS films should be in the paraelectric state to minimize the losses : they are good candidates as the loss tangent of BST may be as low as 6.10^{-3} at 1 MHz and room temperature. For applications in DC or in low frequencies such for infrared or gas sensors, the films should be in the ferroelectric state. A doping with a very low level of tin gives a high yield of usable BTS films and a good reproducibility of their electrical properties. In particular a record tunability of 76 % has been obtained with a BTS film under a DC field of 22.5 V/µm.
Finally, the electrical properties of our optimized doped $BaTiO_3$ (BST and BTS) lead free ferroelectric thin films are comparable to those of PZT films deposited by sol-gel on the same Si/Pt substrates, except for the piezoelectric performances as shown in the following table.

Films	dielectric		ferroelectric			pyroelectric	piezoelectric	
	ε' 1MHz	tg δ 1MHz	Pr (µC/cm²)	Ec (V/µm)	tunability (%)	γ (µC/m²/K)	d_{33} direct (pC/N)	d_{33} inverse (pm/V)
BST	830	0.01	6	4.3	56% @ 12V/µV	350	19	23
PZT	970	0.035	17	5.5	53% @ 25V/µV	200	85	31

Table 1. Comparison of the electrical properties of $Ba_{0.9}Sr_{0.1}TiO_3$ and $PbZr_{0.52}Ti_{0.48}O_3$ films deposited by sol-gel on platinized silicon substrates.

8. Acknowledgment

We would like to thank ADEME and the Conseil Régional Nord-Pas de Calais for the grant given to Manuel Mascot during his Ph.D thesis at the University of Littoral-Côte d'Opale. (Calais, France). We also thank Rachel Desfeux from University of Artois (Lens, France) for the piezoelectric force microscopy measurements and Philippe Belleville from CEA (Le Ripault, France) for the deposition of PZT films by sol-gel on Si/Pt substrates.

9. References

Agarwal, S., Sharma, G.L. & Manchanda, R. (2001). Electrical conduction in (Ba,Sr)TiO_3 thin film MIS capacitor under humid conditions. *Solid State Communications*, Vol. 119, pp. 681-686

Arlt, G., Henning, D. & De With, G. (1985). Dielectric properties of fine-grained barium titanate ceramics. *J. Appl. Phys*, Vol. 58, pp. 1619-1625

Bayer, R.L. & Roundy, C.B. (1972). Pyroelectric coefficient direct measurement technique and application to a nsec response time detector, *Ferroelectrics*, Vol. 3, p. 333-338

Burgnies, L., Vélu, G., Blary, K., Carru, J.-C. & Lippens, D. (2007). Tunability of ferroelectric varactors up to 60 GHz. *Electronics Letters*, Vol. 43, N° 21, pp. 1151-1152

Chang, S.T. & Lee, J.Y. (2002). Electrical conduction mechanism in high-dielectric-constant $Ba_{0.5}Sr_{0.5}TiO_3$ thin films, *App. Phys. Lett.*, Vol. 80, pp. 655-657

Chase, D.R., Chen, L.Y. & York R.A. (2005). Modeling the capactive nonlinearity in thin film BST varactors. *IEEE Trans. Microw. Theory Tech.*, Vol. 53, N° 10, pp. 3215-3220

Cho, Y. W., Choi, S.K. & Venkata Rao, G. (2005). The influence of an extrinsic interfacial layer on the polarization of sputtered $BaTiO_3$ film. *Appl. Phys. Lett.*, Vol. 86, p. 202905

Frayssignes, H., Cheng, B.L., Fantozzi, G. & Button, T.W. (2005). Phase transformation in BST ceramics investigated by internal friction measurements. *Jounal of the European Ceramic Society*, Vol. 25, pp. 3203-3206

Frey, M.H., Xu, Z., Han, P. & Payne, D.A. (1998). The role of interfaces on an apparent grain size effect on the dielectric properties for ferroelectric barium titanate ceramics. *Ferroelectrics*, Vol. 206-207, pp 337-353

Houzet, G., Burgnies, L., Vélu, G., Carru, J.-C. & Lippens, D. (2008). Dispersion and loss of ferroelectric $Ba_{0.5}Sr_{0.5}TiO_3$ thin films up to 110 GHz. *Appl. Phys Lett.*, Vol. 93, p. 053507

Houzet, G., Mélique, X., Lippens, D., Burgnies, L., Vélu, G. & Carru, J.-C. (2010). Microstrip transmission line loaded by split-ring resonators tuned by ferroelectric thin film. *Progress in Electromagnetics Research C*, Vol. 12, pp. 225-236

Hu, W., Yang, C., Zhang, W., Liu, G. & Dong, D. (2006). The diffusion of Pt in BST films on Pt/Ti/SiO2/Si substrate by sol-gel method. *J Sol-Gel Sci. Techn.*, Vol. 39, pp. 293-298

Johnson, K. M. (1962). Variation of dielectric constant with voltage in ferroelectrics and its application to paraelectric devices. *J. Appl. Phys*, Vol. 33, pp 2826-2831

Keyson, D., Volanti, D.P., Cavalcante, L.S., Simoes, A.Z., Souza, I.A., Vasconcelos, J.S., Varela, J.A. & Longo, E. (2007). Domestic microwave oven adapted for fast heat treatment of $Ba_{0.5}Sr_{0.5}(Ti_{0.8}Sn_{0.2})O_3$ powders. *Journal of Materials Processing Technology*, Vol. 189, pp. 316–319

Khalfallaoui, A., Vélu, G., Burgnies, L. & Carru, J.-C. (2010). Characterization of doped BST thin films deposited by sol-gel for tunable microwave devices. *IEEE Trans. Ultrason. Ferroelectr. Freq. Control*, Vol. 57, N° 5, pp. 1029-1033

Lefki, K. & Dormans, G. J. M. (1994). Measurement of piezoelectric coefficients of ferroelectric thin films. *J. Appl. Phys.*, Vol. 76, pp. 1764-1767

Liu, S., Liu, M., Jiang, S., Li, C., Zeng, Y., Huang, Y. & Zhou, D. (2003). Fabrication of SiO_2 doped $Ba_{0.8}Sr_{0.2}TiO_3$ glass ceramic films and the measurement of their pyroelectric coefficient. *Materials Science and Engineering B*, Vol. 99, pp. 511-515

Malic, B., Boerasu, I., Mandeljc, M., Kosec, M., Sherman, V., Yamada, T., Setter, N. & Vakadinovic, M. (2007). Processing and dielectric characterization of $Ba_{0.3}Sr_{0.7}TiO_3$. *Journal of the European Ceramic Society*, Vol. 27, pp. 2945-2948

Mascot, M., Fasquelle, D., Vélu, G., Ferri, A., Desfeux, R., Courcot, L. & Carru, J.-C. (2008). Pyro, ferro and dielectric properties of $Ba_{0.8}Sr_{0.2}TiO_3$ films deposited by sol-gel on platinized silicon substrates. *Ferroelectrics*, Vol. 362, pp. 79-86

Mascot, M. (2009). Ph. D thesis, University of Littoral-Côte d'Opale, Calais, France

Mascot, M., Fasquelle, D. & Carru, J.-C. (2011). Very high tunability of $BaSn_xTi_{1-x}O_3$ ferroelectric thin films deposited by sol-gel. *Functional Materials Letters*, to be published in 2011.

Outzourhit, A., Trefny, J.U., Kito, T. & Yarar, B. (1995). Tunability of dielectric constant of $Ba_{0.1}Sr_{0.9}TiO_3$ ceramics in the paraelectric state. *J. Mater. Res.*, Vol. 10, pp. 1411-1417

Parker, C.B., Maria, J.-P. & Kingon, A.I. (2002). Temperature and thickness dependent permittivity of (Ba, Sr) TiO_3. *Appl. Phys Lett.*, Vol. 81, pp. 340-342.

Pontes, F.M., Longo, E., Leite, E.R. & Varela, J.A. (2001). Study of the dielectric and ferroelectric properties of chemically processed $Ba_xSr_{1-x}TiO_3$ thin films. *Thin Solid Films*, Vol. 386, pp. 91-98

Ren, W., Zhou, H-J., Wu, X.-Q., Zhang, L-Y. & Yao, X. (1997). Measurement of piezoelectric coefficients of lead zirconate titanate thin film by the normal load method using a composite tip. *Materials Letters*, Vol. 31, pp. 185-188

Scott, J.F., Araujo, C.A., Melnick, B.M., Mc Millan, L.D. & Zuleeg, F.L. (1991). Quantitative measurement of space-charge effects in lead zirconate-titanate memories. *J. Appl. Phys.*, Vol. 70, pp. 382-388

Shen, M., Dong, Z., Gan, Z. & Ge, S. (2002). Oxygen-related dielectric relaxation and leakage characteristics of Pt/Ba,Sr.TiO_3/Pt thin-film capacitors, *Appl. Phys. Lett.*, Vol. 80, pp. 2538-2540

Song, S.N., Zhai, J.W. & Yao, X. (2006). The study of the microstructure and tunability of $Ba(Sn_xTi_{1-x})O_3$ thin films. *Integrated Ferroelectrics*, Vol. 78, pp. 337–344

Sun, L.L., Tan, O.K., Liu, W.G., Chen, X.F. & Zhu, W. (2003). Comparaison study on sol-gel $Pb(Zr_{0.3}Ti_{0.7})0_3$ and $Pb(Zr_{0.3}Ti_{0.7})0_3/PbTi0_3$ multilayer thin films for pyroelectric infrared detectors. *Microelectronic Engineering*, Vol. 66, pp. 738-744

Taylor, D. V. & Damjanovic, D. (1998). Domain wall pinning contribution to the nonlinear dielectric permittivity in $PbZrTiO_3$ thin films. *Appl. Phys. Lett*, Vol. 73, pp. 2045-2047

Uchino, K. (2010). *Ferroelectric Devices* (2nd edition), CRC Press, Boca Raton, USA

Vélu, G., Carru, J.-C., Cattan, E., Remiens, D., Mélique, X. & Lippens, D. (2003). Deposition of ferroelectric BST thin films by sol-gel route in view of electronic applications. *Ferroelectrics*, Vol. 288, pp. 59-69

Yang, P., Deng, H. & Chu, J. (1998). Highfield effects of layered perovskite ferroelectric thin films, *Science in China*, Vol. 41, pp. 502-510

Zhang, T. & Ni, H. (2002). Pyroelectric and dielectric properties of sol–gel derived barium–strontium–titanate ($Ba_{0.64}Sr_{0.36}TiO_3$) thin films. *Sensors and Actuators A*, Vol. 100, pp. 252–256

Zhou, C. & Newns, D. M. (1997). Intrinsic dead layer effect and the performance of ferroelectric thin film capacitors. *J. Appl. Phys.*, Vol. 82, pp. 3081-3088

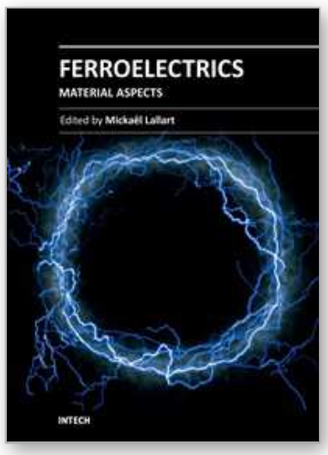

Ferroelectrics - Material Aspects

Edited by Dr. MickaÃ«l Lallart

ISBN 978-953-307-332-3
Hard cover, 518 pages
Publisher InTech
Published online 24, August, 2011
Published in print edition August, 2011

Ferroelectric materials have been and still are widely used in many applications, that have moved from sonar towards breakthrough technologies such as memories or optical devices. This book is a part of a four volume collection (covering material aspects, physical effects, characterization and modeling, and applications) and focuses on ways to obtain high-quality materials exhibiting large ferroelectric activity. The book covers the aspect of material synthesis and growth, doping and composites, lead-free devices, and thin film synthesis. The aim of this book is to provide an up-to-date review of recent scientific findings and recent advances in the field of ferroelectric materials, allowing a deep understanding of the material aspects of ferroelectricity.

InTech Europe
University Campus STeP Ri
Slavka Krautzeka 83/A
51000 Rijeka, Croatia
Phone: +385 (51) 770 447
Fax: +385 (51) 686 166
www.intechopen.com

InTech China
Unit 405, Office Block, Hotel Equatorial Shanghai
No.65, Yan An Road (West), Shanghai, 200040, China
中国上海市延安西路65号上海国际贵都大饭店办公楼405单元
Phone: +86-21-62489820
Fax: +86-21-62489821

IntechOpen